



Construction 0D/2D heterojunction by highly dispersed Ni_2P QDs loaded on the ultrathin $\text{g-C}_3\text{N}_4$ surface towards superhigh photocatalytic and photoelectric performance



Zhiyuan Lu^a, Chunmei Li^b, Juan Han^c, Lei Wang^a, Shuhao Wang^a, Liang Ni^a, Yun Wang^{a,*}

^a School of Chemistry and Chemical Engineering, Jiangsu University, Zhenjiang, 212013, PR China

^b Institute of Green Chemistry and Chemical Technology, School of Chemistry and Chemical Engineering, Jiangsu University, Zhenjiang, 212013, PR China

^c School of Food and Biological Engineering, Jiangsu University, Zhenjiang, 212013, PR China

ARTICLE INFO

Keywords:

0D/2D Heterojunction
 $\text{Ni}_2\text{P}/\text{g-C}_3\text{N}_4$ Composite structure
 Photocatalytic H_2 evolution
 PEC Performance
 Charge separation behavior

ABSTRACT

It is a hot topic to seek cheap and efficient cocatalyst to improve the activity of graphitic carbon nitride ($\text{g-C}_3\text{N}_4$) in photocatalytic water splitting to produce hydrogen and photoelectrochemical (PEC) performance. Herein, we prepared successfully the novel 0D/2D heterojunction by the modification of Ni_2P quantum dots (QDs) as cocatalyst on the surface of ultrathin $\text{g-C}_3\text{N}_4$ layer, which can greatly enhance the photocatalytic hydrogen production and PEC performance under visible light owing to the improvement of separation efficiency of photo-generated charge carriers and visible-light absorption capacity. Surprisingly, the optimum amount of Ni_2P loaded on the $\text{g-C}_3\text{N}_4$ is 3 wt%, whose hydrogen production rate is $1503 \mu\text{mol h}^{-1} \text{g}^{-1}$ being far superior to that of $\text{g-C}_3\text{N}_4$ decorated by 3 wt% Pt ($560 \mu\text{mol h}^{-1} \text{g}^{-1}$). Moreover, the photocurrent response value of $\text{Ni}_2\text{P}/\text{g-C}_3\text{N}_4$ photocatalyst is over 11 times and 3 times that of pure $\text{g-C}_3\text{N}_4$ and Pt/ $\text{g-C}_3\text{N}_4$, respectively. What's better, the stable photocatalytic H_2 evolution and PEC performance of $\text{Ni}_2\text{P}/\text{g-C}_3\text{N}_4$ demonstrates its high stability and reusability resulting from Ni-N coordination on the surface of $\text{g-C}_3\text{N}_4$. This work provides valid evidence for the development of cheap, efficient and durable cocatalyst acting on the $\text{g-C}_3\text{N}_4$, opening up new opportunities and possibilities for dual function application.

1. Introduction

Under the present background of the increasing depletion of fossil fuels, the energy crisis seriously threatens the progress and development of human society. If renewable energy is not timely exploited as a substitute, social science and technology will be unavoidably restrained [1,2]. H_2 is admittedly recognized as renewable and clean energy, particularly significant for relieving global energy demand. Meanwhile, the photoelectrochemical (PEC) performance has also been widely researched in energy field [3]. For this situation, the photocatalytic technology is an effective means to actualize the preparation of hydrogen energy and improvement of photoelectric conversion efficiency, which has multiple advantages of low cost, non-pollution, mild reaction conditions as well as high stability [4]. At present, there have been a large number of literatures about the syntheses of various photocatalysts for enhanced photocatalytic and photoelectric performance [5]. But it is still a huge challenge and groping focus to find efficient, non-toxic, durable catalysts with dual functions such as photocatalysis water splitting for H_2 evolution and PEC performance.

In recent years, $\text{g-C}_3\text{N}_4$ has been widely reported as a commonly used non-metal organic photocatalyst under visible light owing to its suitable bandgap position, excellent stability, convenient preparation methods and so forth [6–10]. However, the photocatalytic and photoelectric activity of pure $\text{g-C}_3\text{N}_4$ is fairly low because of the rapid recombination of photogenerated electron-hole pairs, so it is necessary to construct the $\text{g-C}_3\text{N}_4$ -based composite material. For example, pristine $\text{g-C}_3\text{N}_4$ can be combined with CdS [11], Bi_3TaO_7 [12] or Pt-Co alloy nanoparticle [13] into 2D/0D structure, with NiAl-LDH [14] or CPFA [15] into 2D/2D structure and with CdS/Rgo [16] into 2D/1D/2D structure. The construction of composite structure for $\text{g-C}_3\text{N}_4$ does enhance its photocatalytic hydrogen production performance and photoelectrochemical property, but there is still large space for improvement in terms of separating photon-generated carriers.

As we all know, the microscopic morphology and structure of materials are closely related with their properties, so it has become a common and effective modification method to construct unique compound structure for $\text{g-C}_3\text{N}_4$ [17–26]. Hence, quantum dots (QDs), as semiconductor nanocrystals, have been considered as one of the most

* Corresponding author.

E-mail address: yunwang@ujs.edu.cn (Y. Wang).

potential structures to suppress recombination of photogenerated electron-hole pairs [27–31], settling for practical application in photocatalysis and photoelectricity [32,33]. Briefly speaking, the forceful quantum confinement derived from QDs is propitious to shorten the route length of photoexcited charge transmission [34–39]. On the one hand, faster charge transmission is able to increase hydrogen production rate. On the other hand, QDs may serve as source of photoelectric response to optical excitation. Nonetheless, there are few literatures about QDs modified $g\text{-C}_3\text{N}_4$ composites to improve photocatalytic and photoelectric performance. For instance, B. Babu etc. adopted solvothermal method to make SnO_2 QDs grow on the surface of $g\text{-C}_3\text{N}_4$ [40]; Junqi Li etc. employed oil-in-water self-assembly method to load $\text{Ag}@\text{AgCl}$ QDs on $g\text{-C}_3\text{N}_4$ sheets [41]; Lihua Yao etc. utilized in-situ growth method to anchor $\text{Cd}_{0.5}\text{Zn}_{0.5}\text{S}$ QDs on $g\text{-C}_3\text{N}_4$ microribbons [42]. There is no doubt that the construction of 0D/2D heterostructure of QDs and $g\text{-C}_3\text{N}_4$ are beneficial to efficiently facilitate the activity of as-prepared photocatalyst. Most recently, a kind of transition metal phosphate, i.e. Ni_2P , has become an excellent cocatalyst for electrocatalysis and photocatalysis, inhibiting effectively the recombination of photogenerated charge carriers [43,44]. However, literatures about Ni_2P QDs as co-catalysts of ultrathin $g\text{-C}_3\text{N}_4$ layer have not been reported at present. Hence, it is reasonably conjectured that Ni_2P QDs decorated ultrathin $g\text{-C}_3\text{N}_4$ photocatalyst may tremendously enhance the photocatalytic hydrogen production activity and PEC performance.

In this work, the 0D/2D heterojunction photocatalyst has been successfully prepared by Ni_2P QDs embedded on the surface of ultrathin $g\text{-C}_3\text{N}_4$ layer. Under the same experimental conditions, the photocatalytic hydrogen production and PEC performance of $\text{Ni}_2\text{P}/g\text{-C}_3\text{N}_4$ will be superior to that of $\text{Pt}/g\text{-C}_3\text{N}_4$ with different content of cocatalyst, demonstrating noble-metal-free Ni_2P has the potential to replace the noble metal Pt. What's more, we gained an insight into this unique performance by light absorption, fluorescence and luminescent decay, etc. characterizations that significantly influenced factors on photocatalytic and PEC performance. Accompanied with detailed analyses of reaction mechanism, it is expected that our work will develop important insight on the highly active and low-cost catalyst for multiple applications.

2. Experimental section

2.1. Preparation and characterizations

Urea (AR, 99%), Nickel(II) acetate tetrahydrate ($\text{Ni}(\text{OAc})_2\cdot4\text{H}_2\text{O}$, AR, 99%), NaOH (AR, 99%), NaH_2PO_2 (AR, 99%), $\text{H}_2\text{PtCl}_6\cdot\text{H}_2\text{O}$ (AR, 99%), Triethanolamine (AR, 98%) and N_2 (99.999%). All raw materials were purchased and used without further purification.

Graphitic carbon nitride ($g\text{-C}_3\text{N}_4$) nanosheets were prepared by the thermal polycondensation of urea with some modifications. Briefly, 20 g of urea was dried at 80 °C in the oven overnight. Then, dried urea was ground into powder in the agate mortar and put in a covered crucible. Next, the preprocessed urea was heated at 550 °C for 4 h with a heating rate of 2.5 °C/min. After cooling down, the light yellow product was washed in nitric acid solution ($\text{pH} = 1$) for 12 h, followed by washing with distilled water about 6 times. After being dried thoroughly, the resultant $g\text{-C}_3\text{N}_4$ product was further treated in a muffle furnace at 500 °C for 2 h with a heating rate of 2.5 °C/min.

Subsequently, 200 mg $g\text{-C}_3\text{N}_4$ was well-dispersed in 12 mL of deionized water. A varied amount of $\text{Ni}(\text{OAc})_2\cdot4\text{H}_2\text{O}$ aqueous solution was added dropwise in the above miscible liquid with the mass fraction of Ni loading of 1, 3, 5 or 7%. After the mixed solution stirred for 3 h, a certain amount of NaOH (0.15 M) aqueous solution was added slowly on the basis of the Ni loading with a ratio of Ni: OH at 1:2, followed by magnetic stirring up to 1 h. The resultant mixture was heated at 80 °C with stirring by using an oil bath to evaporate the water. The obtained greenish yellow precursors were completely dried in a vacuum oven. Next, the solid precursor was ground with quantitative NaH_2PO_2 in the

agate mortar until uniformly mixed powder obtained. It was worth noting here that the mole ratio of Ni: NaH_2PO_2 was 1:10. Then, the mixture was placed in a covered crucible and heated in a tube furnace up to 300 °C and maintained for 4 h under N_2 atmosphere. After cooling down to the room temperature, the $\text{Ni}_2\text{P}/g\text{-C}_3\text{N}_4$ products were obtained and then kept in a dryer. Two contrast samples (i.e. Ni_2P and $g\text{-C}_3\text{N}_4$) were prepared through the same procedures. Ni_2P sample was synthesized without adding $g\text{-C}_3\text{N}_4$, while $g\text{-C}_3\text{N}_4$ was prepared without adding $\text{Ni}(\text{OAc})_2\cdot4\text{H}_2\text{O}$ and NaH_2PO_2 . For comparison, $\text{Pt}/g\text{-C}_3\text{N}_4$ was prepared through an in-situ photodeposition method according to previous literatures [45].

X-ray diffraction (XRD) scanned data were collected through a DX-2700 model X-ray diffractometer using Cu Ka radiation at a scan rate of 5°/min in the 2θ range of 10–80°, whose acceleration voltage and current were set at 40 kV and 30 mA, respectively. Fourier transform infrared spectroscopy (FTIR) was performed on a FT-IR Spectrometric Analyzer (Nicolet-560) using KBr powder. Morphology characterizations of the samples were surveyed by transmission electron microscopy (TEM) and high-resolution transmission electron microscopy (HRTEM, JEOL JEM-2100 F). The X-ray photoelectron spectroscopy (XPS) was performed by using a Thermo ESCALAB 250X (America) electron spectrometer using 150 W Al K α X-ray sources and the peak positions were corrected against C 1 s peak (284.6 eV) from the adventitious carbon. UV-vis diffuse reflectance spectra (DRS) were measured on a HITACHI-3900 UV-vis spectrophotometer. The Brunauer-Emmett-Teller (BET) specific surface area was calculated using the adsorption data and the average pore size was determined by the Barret-Joyner-Halenda method. The photoluminescence (PL) spectra and fluorescence decay spectra were recorded on a FLUOROMAX-4C-TCSPEC at room temperature.

2.2. Photocatalytic activity experiments

The photocatalytic reaction was measured in a closed system (total volume about 100 mL). The $\text{Ni}_2\text{P}/g\text{-C}_3\text{N}_4$ catalyst (20 mg) was dispersed in aqueous solution of TEOA (20 vol%, pH = 11.4, 20 mL). Then, the reactor had to be bubbled with Ar gas for 15 min to remove air. A 300 W xenon lamp with a 420 nm cutoff filter was used as the visible light source. The photocatalytic reaction of $\text{Pt}/g\text{-C}_3\text{N}_4$ was conducted under the same condition except beginning with 20 mg $g\text{-C}_3\text{N}_4$ and a unique amount of $\text{H}_2\text{PtCl}_6\cdot\text{H}_2\text{O}$ aqueous solution followed by photodeposition of Pt cocatalyst. The amount of H_2 generated was determined using an online gas chromatography system. The AQE was measured under the same conditions except replacing the 420 nm cutoff filter with a band pass interference filter centered at 400, 420, 450, 500, 550, and 600 nm, respectively, during the 2nd hour of the reaction.

2.3. Photoelectrochemical measurements

The photoelectrochemical properties were measured in the VersaSTAT3 electrochemical working station employing a standard three-compartment cell under visible light assembled by a 300 W Xe lamp with a filter ($\lambda > 420$ nm). The as-prepared photocatalysts on the ITO glass (2 × 2 cm), the Pt plate and Ag/AgCl electrode were employed as the working electrode, counter electrode and the reference electrode, respectively. The above standard three-electrode cell was constituted to study the PEC property.

3. Results and discussion

3.1. Structure and morphology representation of the as-prepared photocatalysts

The structure and composition of the as-prepared photocatalyst are first investigated by XRD characterization. As can be seen in Fig. 1, the pure $g\text{-C}_3\text{N}_4$ has two diffraction peaks at 27.4° and 13.0° corresponding

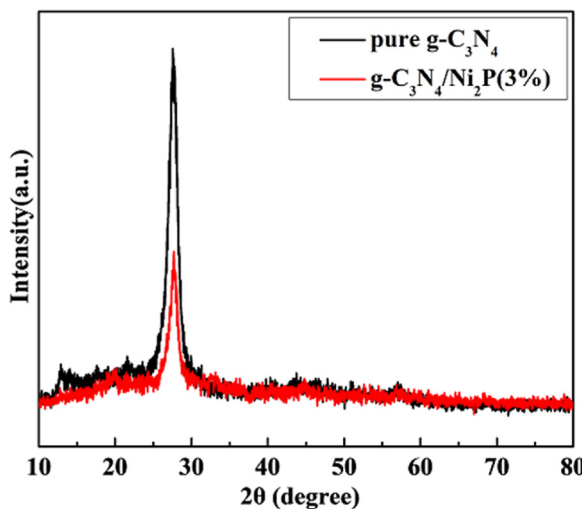


Fig. 1. XRD patterns of pure $\text{g-C}_3\text{N}_4$ and $\text{g-C}_3\text{N}_4/\text{Ni}_2\text{P}$ -3% samples.

to the (002) and (100) planes of $\text{g-C}_3\text{N}_4$ with graphitic structure (JCPDS#87-1526), respectively [46]. Then, the diffraction peak position from $\text{g-C}_3\text{N}_4$ is not obviously changed before and after Ni_2P loading. However, the main diffraction peak of $\text{Ni}_2\text{P}/\text{g-C}_3\text{N}_4$ at 27.4° is pronouncedly weakened, which is potentially due to the structural decoration of Ni_2P QDs on $\text{g-C}_3\text{N}_4$ nanosheets through chemical binding. Noticeably, XRD result reveals that the doped Ni_2P cocatalyst does not incur any impure peaks on the structure of $\text{g-C}_3\text{N}_4$ catalyst, which implies that the Ni element maybe chemically bond with the $\text{g-C}_3\text{N}_4$ catalyst [47]. Moreover, the same XRD characterization method is carried out for $\text{g-C}_3\text{N}_4/\text{Ni}_2\text{P}$ composites with different loading amounts of Ni_2P cocatalyst and similar results are observed (Fig. S1). Nonetheless, with the increasing loading content of Ni_2P , the diffraction peak at 27.4° of $\text{g-C}_3\text{N}_4$ photocatalyst is markedly found to be weaker, which may origin from the Ni-N coordination on the surface of $\text{g-C}_3\text{N}_4$ in agreement with the above analysis.

Fig. S2 reveals fourier transform infrared (FT-IR) spectra of $\text{Ni}_2\text{P}/\text{g-C}_3\text{N}_4$ composites as well as pure $\text{g-C}_3\text{N}_4$. As respect to pure $\text{g-C}_3\text{N}_4$ and $\text{g-C}_3\text{N}_4/\text{Ni}_2\text{P}$, the presence of a wide adsorption band between 800 and 1800 cm^{-1} is related to the polymerization structure of $\text{g-C}_3\text{N}_4$ due to the vibration characteristic of triazine ring and heptazine heterocyclic ring. The wide band ranging from $3000\text{--}3400\text{ cm}^{-1}$ involve uncondensed amino groups ($-\text{NH}$) and hydroxyl group ($-\text{OH}$) of the surface-adsorbed H_2O . In addition, no obvious signal about the formation of $\text{P}-\text{N}$ or $\text{P}-\text{C}$ bond is observed, suggesting that P element is not doped into the structure of $\text{g-C}_3\text{N}_4$. Particularly, similar FT-IR information is also characterized in $\text{g-C}_3\text{N}_4/\text{Ni}_2\text{P}$ photocatalyst with Ni_2P loading, illustrating those $\text{g-C}_3\text{N}_4/\text{Ni}_2\text{P}$ composites maintain the same structure as pure $\text{g-C}_3\text{N}_4$ and no produced other impurity peaks. This result is in great accordance with XRD analysis.

In order to have a thorough insight into the microscopic morphology of $\text{Ni}_2\text{P}/\text{g-C}_3\text{N}_4$ photocatalyst, the microstructural analyses were necessarily performed and the results are shown in Fig. 2. The transmission electron microscopy (TEM) images present the typical 2D nanosheet structure of $\text{g-C}_3\text{N}_4$ (Fig. 2a). It also displays ultrathin structural features observed from the edge of $\text{g-C}_3\text{N}_4$ nanosheet. By contrast, as is shown in the bright and dark field TEM images (Fig. 2b–c), Ni_2P QDs are distinctly observed on the surface of $\text{g-C}_3\text{N}_4$ nanosheets, validating the existence of Ni_2P cocatalyst as sufficient surface active sites. Especially, the sizes of all Ni_2P nanoparticles are smaller than 10 nm. Therein nanoparticles ranging from 4 to 5 nm account for the highest proportion of 30.3%. Additionally, the high resolution TEM (HRTEM) image (Fig. 2d) clearly indicates the close connection between Ni_2P QDs and $\text{g-C}_3\text{N}_4$ nanosheets. The more detailed HRTEM image (Fig. 2e) shows the distinct lattice fringes with an

interplanar spacing of 0.273 nm, which agrees well with the (200) plane of Ni_2P . Lastly, the corresponding elemental mapping images of $\text{Ni}_2\text{P}/\text{g-C}_3\text{N}_4$ photocatalyst (Fig. 2f–i) further confirm the homogeneous distribution of the elements Ni and P on the surface of $\text{g-C}_3\text{N}_4$ catalyst. There is no other obvious compositional distribution among the whole architecture. These results further prove that the Ni_2P QDs has been anchored on the $\text{g-C}_3\text{N}_4$ surface uniformly without generating any impurities, which are in line with the analyses of XRD and FT-IR.

Furthermore, the elements and surface chemical states of photocatalysts were researched by X-ray photoelectron spectroscopy (XPS). The XPS spectra of $\text{g-C}_3\text{N}_4$ and $\text{Ni}_2\text{P}/\text{g-C}_3\text{N}_4$ (Fig. 3a) verified that C, N were the co-owned and predominant elements, while Ni and P were the unique elements of the as-prepared $\text{Ni}_2\text{P}/\text{g-C}_3\text{N}_4$ catalyst, which indicates $\text{Ni}_2\text{P}/\text{g-C}_3\text{N}_4$ photocatalyst has been successfully synthesized. The high-resolution N 1s spectrum of $\text{g-C}_3\text{N}_4$ (Fig. 3b) was decomposed into three peaks at 397.1 eV, 399.0 eV and 403.0 eV, which can be assigned to sp^2 -hybridized nitrogen in triazine rings ($\text{C}-\text{N}=\text{C}$), tertiary nitrogen ($\text{N}-(\text{C})_3$) groups, and positive charge localization in heterocycles ($\text{C}-\text{NH}$), respectively [48]. It is worth noting that the N 1s peak of tertiary nitrogen groups in $\text{Ni}_2\text{P}/\text{g-C}_3\text{N}_4$ located at 398.8 eV decreases by 0.2 eV compared to that in $\text{g-C}_3\text{N}_4$, which implies the combination of chemical bonds between Ni_2P QDs and $\text{g-C}_3\text{N}_4$ layer to form $\text{N}-\text{Ni}$ bond. In contrast, there is no change at the N 1s peak of triazine rings located at 397.1 eV. Therefore, it is believed that Ni element can just interact with N element in tertiary nitrogen groups. More precisely, the electrons in triazine rings from N and C atoms have formed π bonds, not further forming bonds with Ni atoms. In term of Ni 2p spectrum (Fig. 3c), there are two predominant peaks at 855.3 and 874.0 eV corresponding to $\text{Ni } 2\text{p}_{3/2}$ and $\text{Ni } 2\text{p}_{1/2}$ in Ni_2P [49], while the peak at 860.1 eV is just the accompanied peak of $\text{Ni } 2\text{p}_{3/2}$ [50]. Fig. 3d gives the high resolution XPS spectrum of P 2p and the peak at 129.7 eV is a sign of Ni-P bonds [51]. In short, $\text{g-C}_3\text{N}_4$ catalyst has formed chemical bonds with Ni_2P cocatalyst in $\text{Ni}_2\text{P}/\text{g-C}_3\text{N}_4$ composite.

3.2. Photocatalytic and photoelectric performance over the as-prepared photocatalysts

We apply the as-prepared photocatalysts to water splitting for H_2 evolution under visible light. As is vividly illustrated in Fig. 4a, with the loading of Ni_2P on $\text{g-C}_3\text{N}_4$, the H_2 evolution activity of hybrids $\text{Ni}_2\text{P}/\text{g-C}_3\text{N}_4$ have drastically been enhanced ($\lambda > 420\text{ nm}$), while pure $\text{g-C}_3\text{N}_4$ can just produce $12.5\text{ }\mu\text{mol h}^{-1}\text{ g}^{-1}$ of H_2 . Fortunately, with 1% (1 wt% of Ni) of Ni_2P loading, the H_2 evolution rate can be remarkably increased to $1069.5\text{ }\mu\text{mol h}^{-1}\text{ g}^{-1}$. What's better, the H_2 evolution rate of $1503\text{ }\mu\text{mol h}^{-1}\text{ g}^{-1}$ is reached at 3% of Ni loading, which has been the drastically high value reported so far. Nevertheless, the H_2 evolution rate is evidently decreased with higher loadings of Ni_2P , because of the shielding of the light absorption by excess Ni_2P in the reaction system [52]. Noticeably, the highest H_2 evolution rate of $\text{Ni}_2\text{P}/\text{g-C}_3\text{N}_4$ is closely three times that of the optimized Pt/g-C₃N₄ ($560\text{ }\mu\text{mol h}^{-1}\text{ g}^{-1}$). To conclude, the photocatalytic hydrogen production performance of the prepared photocatalyst is improved remarkably superior to Pt/g-C₃N₄ catalyst, claiming that Ni_2P QDs is promising to replace noble metal Pt as cocatalyst of $\text{g-C}_3\text{N}_4$. Additionally, the apparent quantum efficiency (AQE) was measured under the same conditions of the reaction by merely changing band pass filters with different wavelengths. In the Fig. 4b, we can find that both quantum efficiency and optical absorption curve decrease with the increase of light wavelength. A relatively high AQE of 4.8% at 400 nm is achieved by $\text{g-C}_3\text{N}_4/\text{Ni}_2\text{P}$ -3% photocatalyst.

Considering the practical application of $\text{Ni}_2\text{P}/\text{g-C}_3\text{N}_4$ photocatalyst, its stability is also a very crucial factor. As is clearly demonstrated in Fig. 5a, the H_2 generation rate of $\text{Ni}_2\text{P}/\text{g-C}_3\text{N}_4$ displays negligible reduction after five runs, illustrating that $\text{Ni}_2\text{P}/\text{g-C}_3\text{N}_4$ has eminent stability. In order to further confirm the stability and reusability of photocatalyst, the $\text{g-C}_3\text{N}_4/\text{Ni}_2\text{P}$ -3% sample after cyclic reaction was

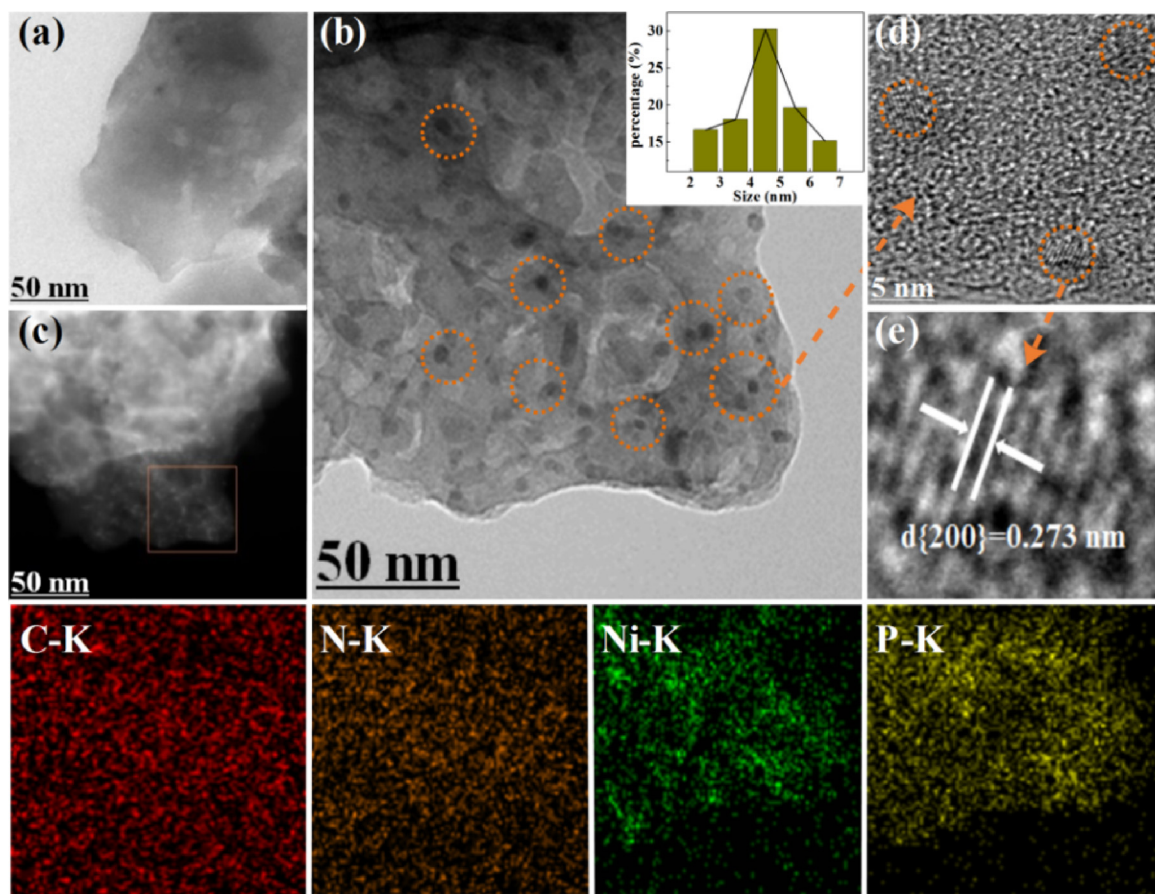


Fig. 2. TEM image of pure g-C₃N₄ (a), Bright field (b) and dark field (c) TEM images of g-C₃N₄/Ni₂P and size distribution (inset of b), HRTEM images (d and e) and STEM-EDX elemental mapping (f–i) of g-C₃N₄/Ni₂P.

characterized again through the transmission electron microscopy (TEM). Obviously, the microstructure of g-C₃N₄/Ni₂P photocatalyst has not been changed at all in Fig. 5b because plenty of Ni₂P QDs are still attached to the surface of the ultrathin g-C₃N₄ nanosheet. All the above results prove the as-prepared 0D/2D photocatalyst can satisfy the condition of practical application because of high stability and reusability.

Besides superhigh hydrogen production performance, PEC properties of as-synthesized Ni₂P/g-C₃N₄ photocatalyst can also be evaluated for practical application. As a main indicator for photoresponse, photocurrent(I) reflects the generation of electron-hole pairs under the irradiation of visible light. Hence, PEC I-t curves are employed to study the interfacial charge separation efficiency and mobility for the photocatalysts under the periodic illumination of 30 s. Seen from Fig. 6a, the measured current value of pristine g-C₃N₄ is 7.48 μA while that of Ni₂P/g-C₃N₄ composite is 82.58 μA under the potential of 0.7 V vs. Ag/AgCl. The photocurrent value of Ni₂P/g-C₃N₄ photocatalyst is over 11 times that of bare g-C₃N₄, which unveils that the photo-reduction and photo-oxidation activity of g-C₃N₄ is drastically boosted for the construction of Ni₂P/g-C₃N₄ heterojunction, benefiting the enhancement of PEC performance. Surprisingly, the current value of Ni₂P/g-C₃N₄ is 3.3 times that of Pt/g-C₃N₄ (25.02 μA), showing the probability of low-cost metals as cocatalysts of g-C₃N₄ in replacement of noble metals in PEC property. Furthermore, the photocurrent formed by the Ni₂P/g-C₃N₄ catalyst is much very stable and durable, beneficial for the practical application. Moreover, EIS measurement can provide the valid evidence for the mobility of electrons at the interfacial of solid electrode, and the results are displayed in Fig. 6b. The diameter of EIS Nyquist plots for g-C₃N₄/Ni₂P is far smaller than pure g-C₃N₄ and Pt/g-C₃N₄, which demonstrates that Ni₂P/g-C₃N₄ photocatalyst possesses less charge

migrate resistance at the interfacial electrolyte solution [53,54], thus displaying the excellent photocatalytic and photoelectric activity.

Fig. 7 shows I-t curves of Ni₂P/g-C₃N₄ composite under various monochromatic light irradiation including 400 nm, 420 nm, 450 nm, 500 nm, 550 nm and 600 nm. In particular, photocurrent response of Ni₂P/g-C₃N₄ is clearly observed at different wavelengths and the obtained results correspond to the information of AQE in Fig. 4b, which reveals the consistency of photocatalytic and photoelectric properties of Ni₂P/g-C₃N₄ photocatalyst. Therefore, 0D/2D heterojunction structure of Ni₂P/g-C₃N₄ composite greatly enhances photoelectric activity and stability of g-C₃N₄ photocatalyst, which is very benefit for practical applications.

3.3. The influence factors of enhanced photocatalytic and photoelectric activity

For investigating the effect of Ni₂P loading on g-C₃N₄ layers, the optical absorption property of Ni₂P/g-C₃N₄ photocatalyst is analyzed by UV-vis DRS. In Fig. 8a, both pure g-C₃N₄ and Ni₂P/g-C₃N₄ photocatalysts have the same absorption edge (426 nm), determining that the bandgap of g-C₃N₄ is not changed at all after modification of Ni₂P and ruling out the doping of Ni and P atoms into g-C₃N₄. To be precise, according to the intercept of the tangents to the plots of $(\text{ch}v)^{1/2}$ vs photon energy, g-C₃N₄ and Ni₂P/g-C₃N₄ have the same energy gap (Eg) value (2.68 eV). As depicted in the Fig. S3, the band gaps measured herein are consistent with the reported literature values (≈ 2.7). Furthermore, the absorption curve of Ni₂P/g-C₃N₄ photocatalyst extends to the visible light range up to about 700 nm, which is helpful to improve photocatalytic activity. This result is also corresponding to the results of AQE and photocurrent under different monochromatic light. In

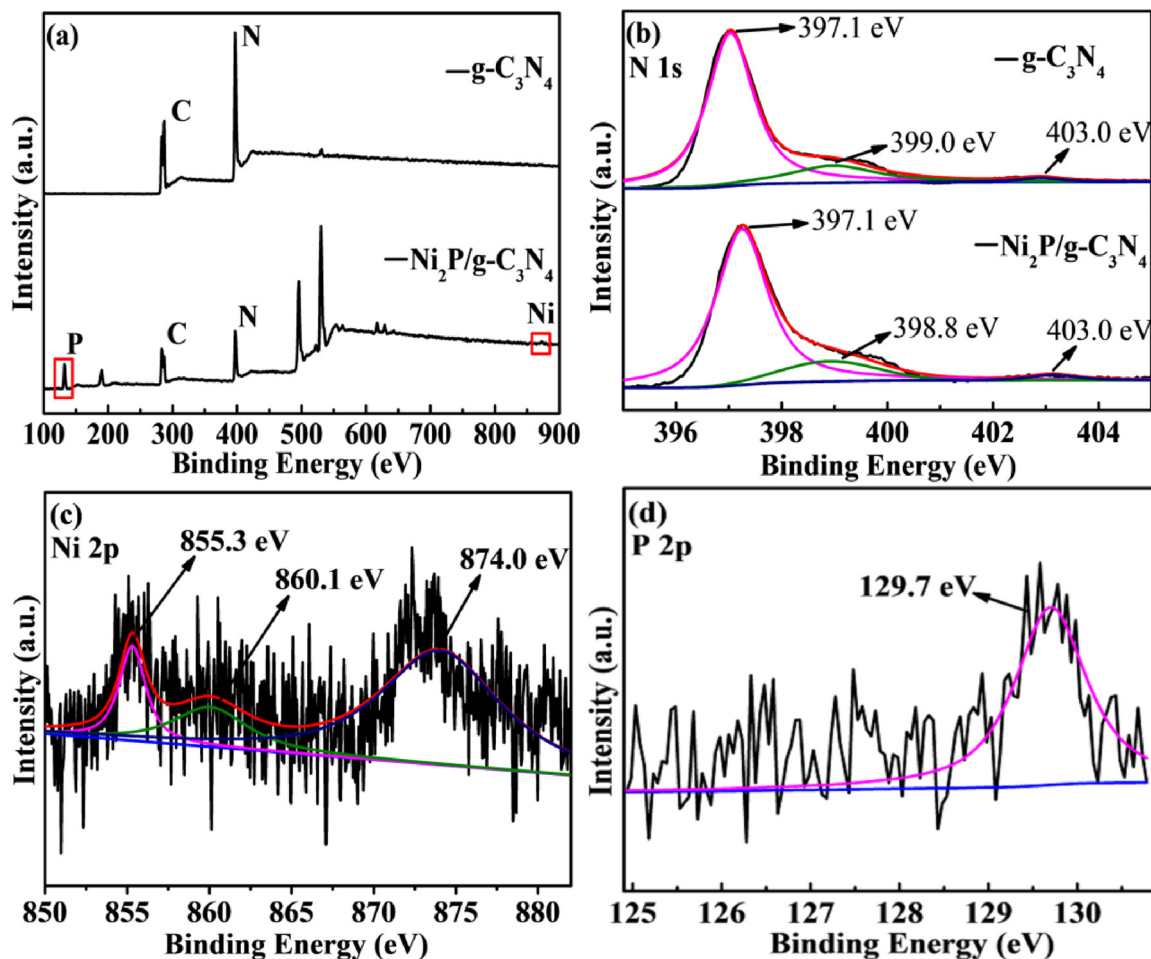


Fig. 3. XPS spectra of g-C₃N₄ and g-C₃N₄/Ni₂P: survey spectrum (a), N 1 s (b), Ni 2p (c) and P 2p (d).

addition, we can find the valence band value of pure g-C₃N₄ is 1.48 eV in Fig. 8b. Amazingly, the VB value (1.10 eV) of g-C₃N₄ in Ni₂P/g-C₃N₄ shifts up 0.38 eV, which implies that the conduction band (CB) value of g-C₃N₄ also has the up-shift owing to the unchanged bandgap value. As a consequence, photocatalytic H₂ production performance and photocurrent response of g-C₃N₄ are obviously enhanced.

In addition, the Brunauer-Emmett-Teller (BET) specific surface area and pore diameter distribution are also the important parameters for photocatalyst. As can be seen in Fig. 9, the hysteresis loops of measured

isotherms appear between 0.4 and 1.0 (P/P₀), which corroborates the presence of mesopores (2–50 nm) in the g-C₃N₄ and Ni₂P/g-C₃N₄ samples. Also, the above consequence is confirmed by pore diameter distributions (inset in Fig. 9) with two peaks of mesoporous. In addition, the specific surface area of Ni₂P/g-C₃N₄ (18.37 m² g⁻¹) is distinctly lower than that of pure g-C₃N₄ (41.1 m² g⁻¹). Therefore, the effects of those factors on improved photocatalytic H₂ generation ability of g-C₃N₄ and Ni₂P/g-C₃N₄ samples are insignificant and neglectful. As a consequence, it further indirectly attests the enhanced

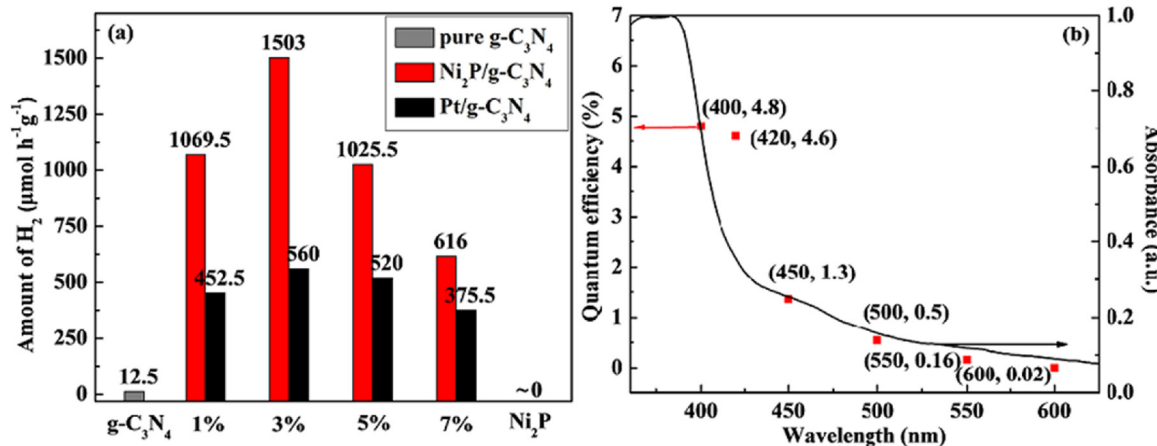


Fig. 4. Photocatalytic H₂ evolution rates over various samples under visible light ($\lambda > 420$ nm) (a); Apparent quantum efficiency and optical absorption curve of Ni₂P/g-C₃N₄ (b).

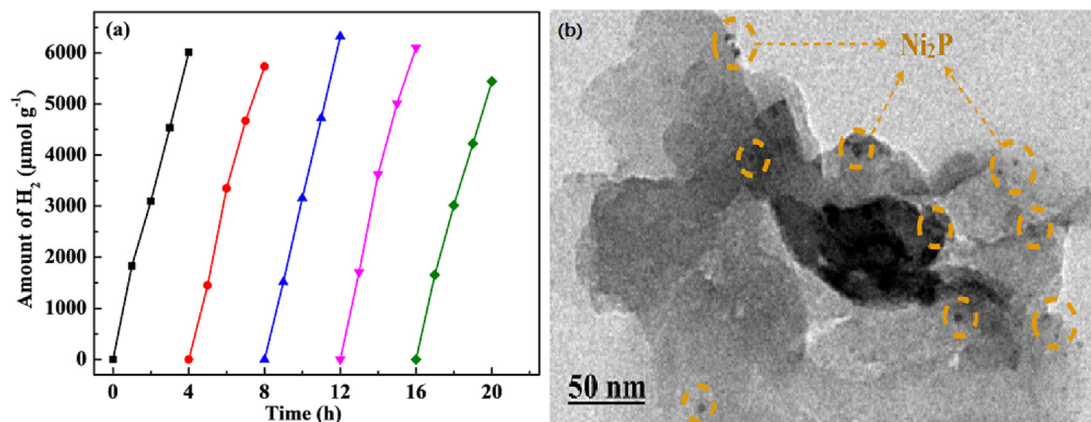


Fig. 5. Time-circle experiment of photocatalytic H₂ evolution over the Ni₂P/g-C₃N₄ sample (a), TEM image of Ni₂P/g-C₃N₄ sample after recycling experiment (b).

photocatalytic activity is ascribed to the effectively transferred and separated efficiency of charge carriers.

Generally speaking, photoluminescence spectra (PL) can reflect the charge separation behavior because higher PL intensity corresponds to lower photocatalytic activity. From Fig. 10a, the PL intensity is descended remarkably at approximately 450 nm after decorating Ni₂P QDs on the g-C₃N₄ surface, resulting in the fast transfer of electrons between g-C₃N₄ and Ni₂P in virtue of Ni-N bonds, which leads to the PL quenching as well as decrease of electron-hole recombination rate. As a result, the improvement of the photon-generated carrier separation efficiency promotes the enhancement of photocatalytic and photoelectric properties. In Fig. 10b, the fluorescent lifetime (1.33 ns) of Ni₂P/g-C₃N₄ is shorter than that (2.58 ns) of pure g-C₃N₄, implying that an additional non-radiative decay channel may be created through the charge separation [55], which is in accordance with our steady-state PL quenching measurements.

3.4. Possible photocatalytic and photoelectric reaction mechanism

Based on the above investigation, the possible mechanism of photocatalysis and photoelectricity of g-C₃N₄/Ni₂P will be analyzed in Fig. 11. Under the visible light irradiation, photo-generated carriers can separate and form electrons and holes in the conduction band (CB) and valence band (VB), respectively. Electrons in the CB are transferred to Ni₂P and react with water to produce hydrogen (H₂). Meanwhile, holes in the VB are neutralized by 20 vol% triethanolamine. With the assist of the Ni₂P cocatalyst, hydrogen production rate of g-C₃N₄ catalyst has been greatly increased. In addition, the photoinduced electrons are

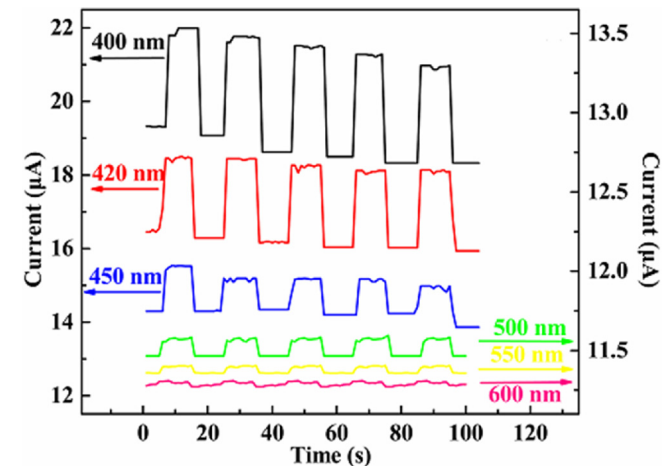


Fig. 7. The periodically illuminated photocurrent – time curves of 3% Ni₂P/g-C₃N₄ at different wavelengths.

transferred efficiently from the g-C₃N₄ to the ITO glass substrate via Ni₂P cocatalyst, and then transferred to the counter electrode (Pt sheet) through the external circuit, triggering the formation of photocurrent (I μA) in PEC tests. The photocurrent enhancement of g-C₃N₄/Ni₂P is ascribed to the high separation efficiency of the photoexcited electron-hole pairs after Ni₂P QDs loading. The formation of nickel-nitrogen bond (Ni-N) firmly fix Ni₂P QDs on the surface of g-C₃N₄ layers, enormously improving light absorption and efficiently boosting the

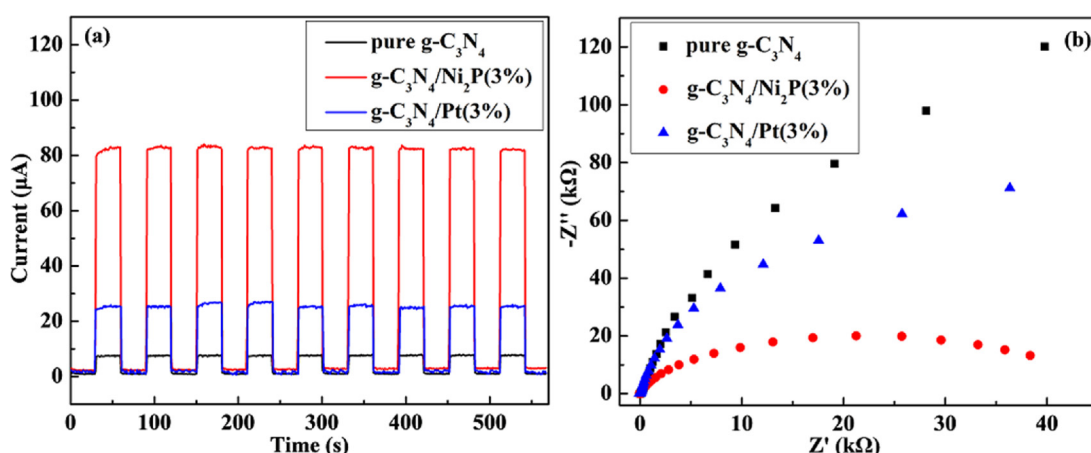


Fig. 6. The transient photocurrent – time (I – t) responses (a) and EIS Nyquist plots (b) of pure g-C₃N₄, g-C₃N₄/Ni₂P-3% and g-C₃N₄/Pt-3% in 0.5 M Na₂SO₄ solution.

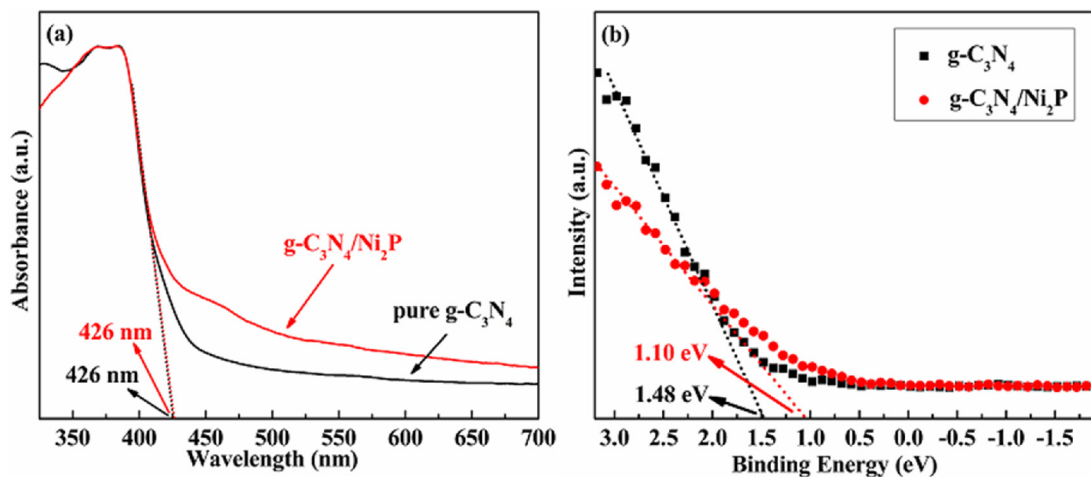


Fig. 8. UV-vis DRS spectra (a) and XPS valence band spectra (b) of $\text{g-C}_3\text{N}_4$ and $\text{g-C}_3\text{N}_4/\text{Ni}_2\text{P}$ -3% samples.

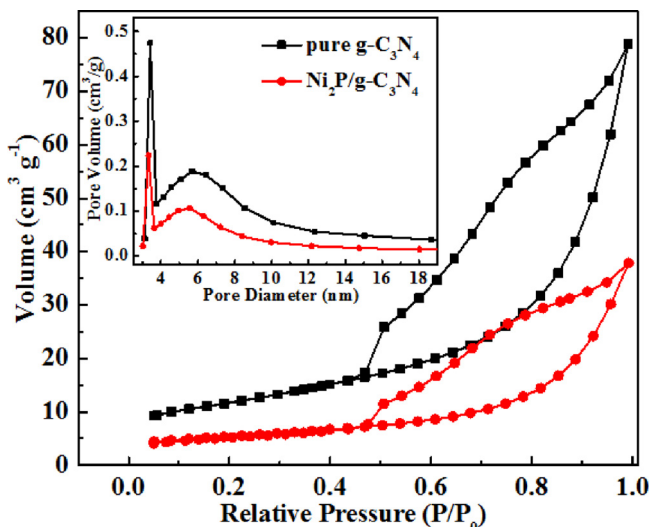


Fig. 9. N_2 adsorption–desorption curves and pore diameter distributions (inset) of pure $\text{g-C}_3\text{N}_4$ and $\text{Ni}_2\text{P}/\text{g-C}_3\text{N}_4$ samples.

separation of photogenerated electron-hole pairs, which enhances both H_2 evolution and PEC performance.

4. Conclusions

In conclusion, noble-metal-free Ni_2P QDs modified $\text{g-C}_3\text{N}_4$ is successfully prepared serving as a low-cost, stable and efficient catalyst for photocatalysis and photoelectricity. Noticeably, $\text{g-C}_3\text{N}_4/\text{Ni}_2\text{P}$ -3% owns the extremely high H_2 evolution rate ($1503 \mu\text{mol h}^{-1} \text{g}^{-1}$) and photocurrent response value ($82.58 \mu\text{A}$), which are more about 120 times and 11 times than that of pure $\text{g-C}_3\text{N}_4$, respectively. Moreover, the photocatalytic and photoelectric activity of $\text{Ni}_2\text{P}/\text{g-C}_3\text{N}_4$ hybrid is approximately 3 times that of the optimized $\text{Pt}/\text{g-C}_3\text{N}_4$, demonstrating transition metal phosphide is desired to become efficient and cheap cocatalyst in replacement of noble metal. The photocatalytic and photoelectric activity of $\text{g-C}_3\text{N}_4$ drastically boosted results from the effective transferred and separated of charge carriers. In addition, the synthesized $\text{g-C}_3\text{N}_4/\text{Ni}_2\text{P}$ has been validated to have quite high stability during recycling tests. This work will provide a significant step toward for developing high-efficiency dual functional catalytic materials utilizing low-cost and sufficient elements (C, N, P and Ni) in the world.

Acknowledgments

This work was supported by the National Natural Science Foundation of China (21606114, 31470434), the Natural Science Fund of Jiangsu Province (BK20150536), the Postdoctoral Science

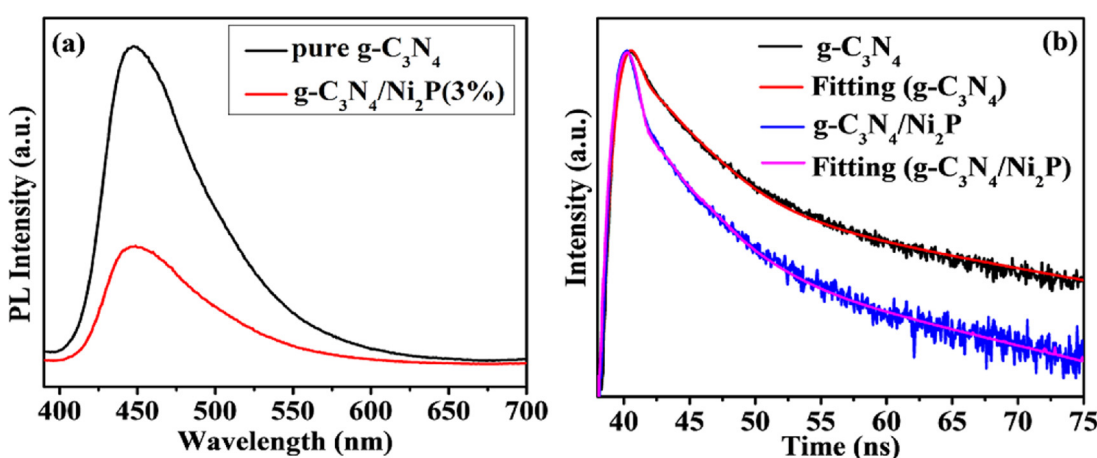


Fig. 10. Photoluminescence spectra (a) and fluorescence decay curves (b) of pure $\text{g-C}_3\text{N}_4$ and $\text{g-C}_3\text{N}_4/\text{Ni}_2\text{P}$ -3% samples.

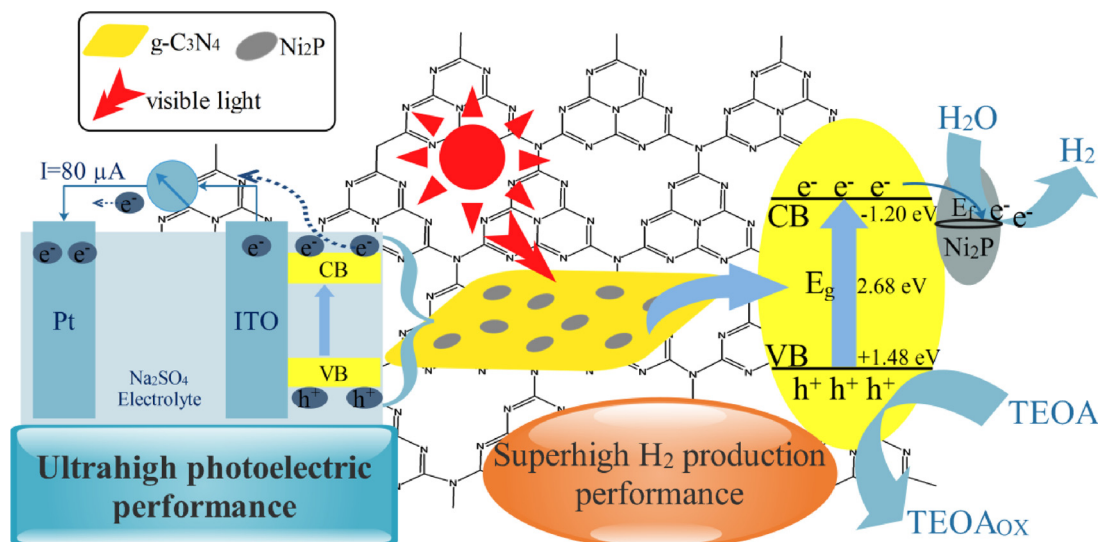


Fig. 11. The possible schematic diagram of photocatalysis and photoelectricity over g-C₃N₄/Ni₂P-3% samples.

Foundation of China (2017M611712, 2017M611717).

Appendix A. Supplementary data

Supplementary material related to this article can be found, in the online version, at doi:<https://doi.org/10.1016/j.apcatb.2018.06.062>.

References

- [1] K.H. Liu, H.X. Zhong, S.J. Li, Y.X. Duan, M.M. Shi, X.B. Zhang, J.M. Yan, Q. Jiang, Progr. Mater. Sci. 92 (2018) 64–111.
- [2] C.M. Li, Y. Xu, W.G. Tu, G. Chen, R. Xu, Green Chem. 19 (2017) 882–899.
- [3] H. Zeng, S. Liu, B. Chai, D. Cao, Y. Wang, X. Zhao, Environ. Sci. Technol. 50 (2016) 6459–6466.
- [4] Y.P. Xie, Z.B. Yu, G. Liu, X.L. Ma, H.M. Cheng, Energy Environ. Sci. 7 (2014) 1895.
- [5] Z.Y. Min, S.Y. Liu, Z.B. He, Asian J. Chem. 26 (2014) 5447–5452.
- [6] J.S. Cheng, Z. Hu, K.L. Lv, X.F. Wu, Q. Li, Y.H. Li, X.F. Li, J. Sun, Appl. Catal. B Environ. 232 (2018) 330–339.
- [7] C.M. Li, G. Chen, J.X. Sun, J.C. Rao, Z.H. Han, Y.D. Hu, Y.S. Zhou, ACS Appl. Mater. Inter. 7 (2015) 25716–25724.
- [8] Y.H. Jiang, P.P. Liu, Y.C. Chen, Z.Z. Zhou, H.J. Yang, Y.Z. Hong, F. Li, L. Ni, Y.S. Yan, Appl. Surf. Sci. 391 (2017) 392–403.
- [9] C.M. Li, G. Chen, J.X. Sun, Y.J. Feng, J.J. Liu, H.J. Dong, Appl. Catal. B Environ. 163 (2015) 415–423.
- [10] Y.H. Li, W.K. Ho, K.L. Lv, B.C. Zhu, S.C. Lee, Appl. Surf. Sci. 430 (2018) 380–389.
- [11] L. Ge, F. Zuo, J.K. Liu, Q. Ma, C. Wang, D.Z. Sun, P.Y. Feng, J. Phys. Chem. C 116 (2012) 13708–13714.
- [12] K. Wang, G.K. Zhang, J. Li, Y. Li, X.Y. Wu, ACS Appl. Mater. Inter. 9 (2017) 43704–43715.
- [13] C. Han, Y. Lu, J. Zhang, L. Ge, Y. Li, J. Mater. Chem. A 3 (2015) 23274–23282.
- [14] S. Tonda, S. Kumar, M. Bhardwaj, P. Yadav, S. Ogale, ACS Appl. Mater. Inter. 10 (2018) 2667.
- [15] Y.H. Jiang, P.P. Liu, Y. Liu, X.F. Liu, F. Li, L. Ni, Y.S. Yan, P.W. Huo, Sep. Purif. Technol. 170 (2016) 10–21.
- [16] S. Tonda, S. Kumar, Y. Gawli, M. Bhardwaj, S. Ogale, Int. J. Hydrog. Energy 42 (2017) 5971–5984.
- [17] Z.Y. Lu, X.X. Zhao, Z. Zhu, M.S. Song, N.L. Gao, Y.S. Wang, Z.F. Ma, W.D. Shi, Y.S. Yan, H.J. Dong, Catal. Sci. Technol. 6 (2016) 6513–6524.
- [18] C.B. Liu, J.B. Chen, H.N. Che, K. Huang, P.A. Charpentier, W.Z. Xu, W.D. Shi, H.J. Dong, RSC Adv. 14 (2017) 8429–8442.
- [19] H.N. Che, J.B. Chen, K. Huang, W. Hu, H. Hu, X.T. Liu, G.B. Che, C.B. Liu, W.D. Shi, J. Alloy. Compd. 288 (2016) 882–890.
- [20] H.N. Che, C.B. Liu, W. Hu, H. Hu, J.Q. Li, J.Y. Dou, W.D. Shi, C.M. Li, H.J. Dong, Catal. Sci. Technol. 8 (2018) 622–631.
- [21] X.X. Zhao, Z.Y. Lu, M.B. Wei, M.H. Zhang, H.J. Dong, C.W. Yi, R. Ji, Y.S. Yan, Appl. Catal. B Environ. 220 (2018) 137–147.
- [22] Z. Zhu, Z.Y. Lu, D.D. Wang, X. Tang, Y.Y. Yan, W.D. Shi, Y.S. Wang, N.L. Gao, X. Yao, H.J. Dong, Appl. Catal. B Environ. 182 (2016) 115–122.
- [23] Y.H. Jiang, P.P. Liu, S.J. Tian, Y. Liu, Z.Y. Peng, F. Li, L. Ni, Z.C. Liu, J. Taiwan Inst. Chem. E 78 (2017) 517–529.
- [24] C.M. Li, G. Chen, J.X. Sun, J.C. Rao, Z.H. Han, Y.D. Hu, W.N. Xing, C.M. Zhang, Appl. Catal. B Environ. 188 (2016) 39–47.
- [25] Y.H. Li, K.L. Lv, W.K. Ho, Z.W. Zhao, Y. Huang, Chin. J. Catal. 38 (2017) 321–329.
- [26] S. Fang, K.L. Lv, Q. Li, H.P. Ye, D.Y. Du, M. Li, Appl. Surf. Sci. 358 (2015) 336–342.
- [27] S. Fang, Y. Xia, K.L. Lv, Q. Li, J. Sun, M. Li, Appl. Catal. B Environ. 185 (2016) 225–232.
- [28] M. Yan, F.F. Zhu, W. Gu, L. Sun, W.D. Shi, Y.Q. Hua, RSC Adv. 6 (2016) 61162–61174.
- [29] S. Yu, Y.Q. Zhong, B.Q. Yu, S.Y. Cai, L.Z. Wu, Y. Zhou, Chem. Phys. 18 (2016) 20338–20344.
- [30] Y.H. Li, K.L. Lv, W.K. Ho, F. Dong, X.F. Wu, Y. Xia, Appl. Catal. B Environ. 202 (2017) 611–619.
- [31] Z.C. Lian, W.C. Wang, S.N. Xiao, X. Li, Y.Y. Cui, D.Q. Zhang, Sci. Rep. 5 (2015) 10461.
- [32] R. Liu, H. Huang, H. Li, Y. Liu, J. Zhong, Y. Li, S. Zhang, Z. Kang, ACS Catal. 4 (2014) 328–336.
- [33] L. Amirav, A.P. Alivisatos, J. Am. Chem. Soc. 132 (2010) 9997–9999.
- [34] M. Shein, R. Nadiv, M. Buzaglo, K. Kahil, O. Regev, Chem. Mater. 27 (2015) 2100–2106.
- [35] F. Liu, M.H. Jang, H.D. Ha, J.H. Kim, Y.H. Cho, T.S. Seo, Adv. Mater. 25 (2013) 3657–3662.
- [36] Z.Y. Jin, Q.T. Zhang, L. Hu, J.Q. Chen, X. Cheng, Y.J. Zeng, Appl. Catal. B Environ. 205 (2017) 569–575.
- [37] H.P. Li, Z. Su, S.Y. Hu, Y.W. Yan, Appl. Catal. B Environ. 207 (2017) 134–142.
- [38] Z.A. Huang, Q. Sun, K.L. Lv, Z.H. Zhang, M. Li, B. Li, Appl. Catal. B Environ. 164 (2015) 420–427.
- [39] Q.Q. Meng, Y.S. Zhou, G. Chen, Y.D. Hu, C.D. Lv, L.S. Qiang, Chem. Eng. J. 334 (2018) 334–343.
- [40] B. Babu, M.Y. Cho, C. Byon, J. Shim, Mater. Lett. 212 (2018) 327–331.
- [41] J.Q. Li, H.J. Hao, J. Zhou, W.J. Li, N. Lei, L. Guo, Appl. Surf. Sci. 422 (2017) 626–637.
- [42] L.H. Yao, D. Wei, Y.M. Ni, D.P. Yan, C.W. Hu, Nano. Energy 26 (2016) 248–256.
- [43] P. Ye, X.L. Liu, J. Iocozzia, Y.P. Yuan, L.N. Gu, G.S. Xu, Z.Q. Lin, J. Mater. Chem. A 5 (2017) 8493–8498.
- [44] W.J. Wang, T.C. An, G.Y. Li, D.H. Xia, H.J. Zhao, Appl. Catal. B Environ. 217 (2017) 570–580.
- [45] J. Hong, X. Xia, Y. Wang, R. Xu, J. Mater. Chem. 22 (2012) 15006.
- [46] M.K. Bhunia, K. Yamauchi, K. Takanabe, Angew. Chem. 53 (2014) 11001.
- [47] M.Q. Wang, W.H. Yang, H.H. Wang, C. Chen, Z.Y. Zhou, S.G. Sun, ACS Catal. 4 (2014) 3928–3936.
- [48] J.S. Zhang, M.W. Zhang, G.G. Zhang, X.C. Wang, ACS Catal. 2 (2012) 940–948.
- [49] H. Zhao, S.N. Sun, P.P. Jiang, Z.C. Xu, Chem. Eng. J. 315 (2017) 296–303.
- [50] J.D. Hong, Y.S. Wang, Y.B. Wang, W. Zhang, R. Xu, ChemSusChem 6 (2013) 2263–2268.
- [51] Z. Pu, Q. Liu, C. Tang, A.M. Asiri, X. Sun, Nanoscale 6 (2014) 11031–11034.
- [52] C.M. Li, Y.H. Du, D.P. Wang, S.M. Yin, W.G. Tu, Z. Chen, M. Kraft, G. Chen, R. Xu, Adv. Funct. Mater. (2017) 4328160.
- [53] B. Chai, J. Yan, C. Wang, Z. Ren, Y. Zhu, Appl. Surf. Sci. 391 (2017) 376–383.
- [54] J. Wang, W. Zhang, Electrochim. Acta 71 (2012) 10–16.
- [55] Z. Sun, H. Zheng, J. Li, P. Du, Energy Environ. Sci. 8 (2015) 2668.